Quenching of Spin Polarization Switching in Organic Multiferroic Tunnel Junctions by Ferroelectric "Ailing-Channel" in Organic Barrier

Shiheng Liang, Zhongwei Yu, Xavier Devaux, Anthony Ferri, Weichuan Huang, Huaiwen Yang, Rachel Desfeux, Xiaoguang Li, Sylvie Migot, Debapriya Chaudhuri, et al.

Quenching of Spin Polarization Switching in Organic Multiferroic Tunnel Junctions by Ferroelectric "Ailing-Channel" in Organic Barrier

Shiheng Liang[1,2], Zhongwei Yu[1,7], Xavier Devaux[1], Anthony Ferri[3], Weichuan Huang[4], Huaiwen Yang[1], Rachel Desfeux[3], Xiaoguang Li[4], Sylvie Migot[1], Debapriya Chaudhuri[5], Hongxin Yang[6], Mairbek Chshiev[5], Changping Yang[2], Bin Zhou[2], Jinghuai Fang[7], Stéphane Mangin[1] and Yuan Lu[1*]

[1]*Institut Jean Lamour, UMR 7198, CNRS-Université de Lorraine, Campus ARTEM, 2 Allée André Guinier, BP 50840, 54011 Nancy, France*

[2]*Department of Physics, Hubei University, Wuhan 430062, P. R. China*

[3]*Univ. Artois, CNRS, Centrale Lille, ENSCL, Univ. Lille, UMR 8181, Unité de Catalyse et Chimie du Solide (UCCS), F-62300 Lens, France*

[4]*Hefei National Laboratory for Physical Sciences at Microscale, Department of Physics, University of Science and Technology of China, Hefei 230026, P. R. China*

[5]*Univ. Grenoble Alpes, INAC-SPINTEC, F-38000 Grenoble, France; CEA, INAC-SPINTEC, F-38000 Grenoble, France; CNRS, SPINTEC F-38000 Grenoble, France*

[6]*Key Laboratory of Magnetic Materials and Devices, Ningbo Institute of Materials Technology and Engineering, Chinese Academy of Sciences, Ningbo, 315201, China*

[7]*School of Science, Nantong University, 9 Seyuan Road, Nantong 226019, P. R. China*

** Corresponding author: yuan.lu@univ-lorraine.fr*

Keywords: organic multiferroic tunnel junctions, spinterface, tunneling magneto-resistance, spin polarization

ABSTRACT:

The ferroelectric control of spin-polarization at ferromagnet (FM)/ferroelectric organic (FE-Org) interface by electrically switching the ferroelectric polarization of the FE-Org has been recently realized in the organic multiferroic tunnel junctions (OMFTJ) and gained intensive interests for future multifunctional organic spintronic applications. Here, we report the evidence of ferroelectric "ailing-channel" in the organic barrier which can effectively pin the ferroelectric domain, resulting in nonswitchable spin polarization at the FM/FE-Org interface. In particular, OMFTJs based on $La_{0.6}Sr_{0.4}MnO_3$/P(VDF-TrFE) (*t*)/Co/Au structures with different P(VDF-TrFE) thickness (*t*) were fabricated. The combined advanced electron microscopy and spectroscopy studies clearly reveal that very limited Co diffusion exists in the P(VDF-TrFE) organic barrier when the Au/Co electrode is deposited around 80K. Pot-hole structures at the boundary between the P(VDF-

TrFE) needle-like grains are evidenced to induce “ailing-channels” that hinder efficient ferroelectric polarization of the organic barrier and result in the quenching of the spin polarization switching at Co/P(VDF-TrFE) interface. Furthermore, the spin diffusion length in the negatively polarized P(VDF-TrFE) is measured to be about 7.2nm at 20K. The evidence of the mechanism of ferroelectric “ailing-channels” is of essential importance to improve the performance of OMFTJ and master the key condition for an efficient ferroelectric control of the spin polarization of “spinterface”.

The organic multiferroic tunnel junctions (OMFTJs)[1,2,3] have recently attracted much attention since they combine advantages of spintronics, organic electronics, and ferroelectric electronics. In comparison to inorganic based devices, organic materials are appealing because of the long spin lifetime of charge carriers,[4] low cost, and chemical diversity.[5,6] In an OMFTJ, the core structure comprises a ferroelectric organic (FE-Org) tunnel barrier layer sandwiched between two ferromagnetic (FM) electrodes. Owing to the combined tunneling magnetoresistance (TMR) and tunneling electroresistance (TER) effects,[7,8,9,10,11,12,13] it shows a performance of a four resistance states.[3] More interestingly, it has been demonstrated that the spin-polarization at the FM/FE-Org interface, called as "spinterface", can be inversed by electrically switching the ferroelectric polarization of the FE-Org.[3] This discovery emphasizes the critical role of "spinterface"[14,15,16,17] on the determination of the spin polarization at organic/ferromagnetic interface and open new functionality in controlling the injection of spin polarization into organic materials via the ferroelectric polarization of the barrier. Despite much effort, direct observations of the FM/FE-Org interfaces and investigation of the influence of FE-Org ferroelectricity on the spin-transport properties governed by the "spinterface" are largely insufficient and remain elusive.

The ferroelectric organic P(VDF-TrFE) material[18,19,20,21] exhibits good piezoelectric and pyroelectric responses as well as low acoustic impedance which matches water and human skin. In the PVDF based ferroelectric tunnel junctions (FTJs) of Au/PVDF/W,[22] 1000% TER at room temperature (RT) has been achieved. In this work, OMFTJs based on $La_{0.6}Sr_{0.4}MnO_3$/P(VDF-TrFE)(t)/Co structures with different thickness, t, of P(VDF-TrFE) were fabricated. By combining scanning transmission electron microscopy (STEM) and electron energy loss spectroscopy (EELS), we investigate the local chemical composition of the structures, especially to understand the stability of the layers, and check the presence of "dead layers" in the organic layer due to the metal diffusion. A mechanism of the ferroelectric "ailing-channels" that hinders the efficient ferroelectric polarization of the organic barrier and consequently quenches the spin polarization

switching at FM/FE-Org interface was evidenced. The understanding of the microstructure influence is of essential importance for the improvement of the OMFTJ device performance and mastering the key conditions for the ferroelectric control of the spin polarization of the "spinterface".

Results and discussions.

Interface morphology and chemistry study by STEM combined with EELS.

OMFTJ samples based on $La_{0.6}Sr_{0.4}MnO_3$/P(VDF-TrFE)(*t*)/Co/Au structure on $SrTiO_3$ substrate were prepared. Different thicknesses of P(VDF-TrFE) (15nm, 19nm and 33nm) are used as tunneling barrier layer. Hereafter, we call them as *thin* (15nm), *medium* (19nm) and *thick* (33nm) sample, respectively. Figure 1a shows a high-angle annular dark-field (HAADF) STEM image of the *thin* sample. The bottom $La_{0.6}Sr_{0.4}MnO_3$ (LSMO) magnetic electrode reveals a good homogeneity with a thickness of 85 nm and low roughness of about 3 nm. However, the P(VDF-TrFE) barrier with a mean thickness of 15 nm appears rough with a peak-to-peak roughness of about 8 nm (zoomed in Figure 1d). Some "pot-hole" structures are found in the organic barrier (indicated with red arrows). The surface morphology of P(VDF-TrFE) barrier is also investigated by atomic force microscopy (AFM) and it reveals a root-mean-square (RMS) roughness of 2.1 nm in the 1×1 μm² window (Figure 1b). The surface morphology exhibits a needle-like crystallite feature with a width of about 50 nm and length of about 100 nm, which is a characteristic of the ferroelectric β phase of P(VDF-TrFE).[23] Figure 1c shows the section profile extracted from the AFM image (marked with the blue line on Figure 1b), which is compared with the profile of the Co/P(VDF-TrFE) interface from the HAADF STEM image (Figure 1d) recorded on the cross section of the film. The very good agreement between the two profiles proves that no modification of the sample morphology occurs during the preparation of the lamella for the STEM observation by focus ion beam (FIB) lift out method. The "pot-hole" structure observed in the STEM image can then be understood to be formed at the boundary of P(VDF-TrFE) needle-like grains. In Figure 1e, we present STEM image of the OMFTJ stack structure with *medium* thickness of P(VDF-TrFE). Compared to the *thin* sample,

the thickness of the organic barrier of the *medium* sample appears much homogenous with a lower roughness about 5 nm. No obvious "pot-hole" structure is found in the observed region.

In the previous works reported on the organic magnetic tunnel junctions based on soft organic materials, such as Alq_3[24,25,26], buckminsterfullerene[16] and P(NDI2OD-T2)[27], it is noteworthy that there exists the penetration of chemical elements from the top metallic electrode into the soft organic layer, leading to a "ill-defined" organic spacer to modify the spin transport properties.[28] In order to examine the chemical diffusion issue in our OMFTJ, HAADF STEM imaging coupled to high spatial resolution STEM-EELS was employed to characterize the chemical distribution at the FM/FE-Org interface. Figure 2a displays the ADF STEM image of the interfacial structure of the *thin* device. One can distinguish some grey contrast zones between the Co and P(VDF-TrFE) layers and also between the P(VDF-TrFE) and LSMO layers (indicated with blue arrows). These grey zones are due to the roughness of Co/P(VDF-TrFE) and P(VDF-TrFE)/LSMO interfaces. Since the lamella prepared by FIB has a certain thickness, the grey zone is a result of the superposition of Co-P(VDF-TrFE) or P(VDF-TrFE)-LSMO layers. EELS spectrum images are registered in the area where the apparent superposition of phases is minimum (area marked with blue rectangle in Figure 2a). The chemical maps resulted from this analysis are presented in Figure 2b. The maps of chemical elements Co (sky-blue), C (red) and La (magenta) are extracted from the EELS spectrum images by using signals of Co_{L3}(779eV), C_K(280eV) and La_{M5}(820eV) edges, respectively. The irregular aspect of the interfaces in the resulting chemical maps is due to the drift correction when recording the spectrum image. Despite the drift, it appears clearly that there is quite limited Co diffusion inside the organic barrier. Since the large roughness of organic barrier is due to the needle like grains of P(VDF-TrFE), one may suppose that the Co diffusion could happen in the grain boundaries. To clarify this point, zones where grains form a "pot-hole" structure are studied (Figure 2c). EELS spectra were recorded crossing the P(VDF-TrFE) layer where Co and P(VDF-TrFE) are superposed. Figure 2d and 2e present the EELS spectra recorded on the positions 1 to 5 marked in the Figure 2c. One can follow

the intensity of $Co_{L3,2}$ and C_k peaks. Although strong peaks of $Co_{L3,2}$ exist in the superposition zone (No.2, blue line), Co signals disappear at the end of this zone, indicating pure P(VDF-TrFE) layer in the boundary zone (No.3, purple line). This clearly confirms that the Co diffusion is also very limited in the grain boundaries in the P(VDF-TrFE) barrier. More structure and chemistry analysis of the *thin* and *medium* samples can be found in Supporting Information S2 and S3.

This result is quite surprising compared to the reported diffusion of metals into the organic layer.[16,24,27] The absence of the Co diffusion into the P(VDF-TrFE) can be a result of the growth of the Au/Co electrode at low temperature (~80K) (please see Supporting Information S1). For comparison, we also fabricated one sample in which the Au/Co electrode was deposited at room temperature. Figure 3 shows the STEM image and corresponding EELS maps of different elements in the area marked with the blue rectangular in Figure 3a. We can observe a grey layer indicated with the yellow arrow in the STEM image (Figure 3a). This layer is homogeneously following the surface morphology of P(VDF-TrFE) and has an almost constant thickness of about 5nm, which is obviously different from the above-mentioned character of the superposition zone due to the interface roughness effect. Moreover, the EELS maps reveal that Co and C coexist in this zone (Figure 3b). Therefore, it can be identified to be the Co inter-diffusion region to form the "ill-defined" dead layer, as reported in many literatures.[16,24,27] The recent work by Subedi *et al.* also reported TMR in LSMO/P(VDF-TrFE)/Co junction.[29] However, their TMR sign cannot be modulated with changing the ferroelectric polarization of the organic barrier. Since their Ag/Co electrode was deposited at RT, this induces a quite large Co diffusion into the Co/P(VDF-TrFE) interface and thus the spin polarization switching at the spinterface is quenched. The direct observation of the FM/FE-Org interfaces proves that the low temperature metal deposition technique can greatly suppress the metal diffusion in the organic barrier, which will be of great interest for the organic electronics community.

Ferroelectric properties studied by PFM.

Like PVDF system, the ferroelectric order of P(VDF-TrFE) copolymer also originates from the permanent dipoles and the cooperative long-range rotation of the molecular chains via the short-range Van der Waals interactions.[3] Two polarization states associated with either F-C-H/Co or H-C-F/Co interface are possible (Inset of Figure 5b). The ferroelectric properties of the P(VDF-TrFE) barrier have been characterized by the piezo-response force microscopy (PFM) at room temperature. Figure 4a displays the local PFM phase and amplitude hysteresis loops recorded on the *thin* P(VDF-TrFE) surface. The local switching behavior and the electromechanical activity are revealed by the two opposite polarization states and the clear hysteresis loops. The coercivities of the polarizing voltage (V_C) in the phase and amplitude loops are found to be identical and as large as 0.5V (average value of the positive and negative polarizations). Furthermore, we plot the dependence of V_C on the P(VDF-TrFE) thickness t in Figure 4b. It is found that the thicker P(VDF-TrFE) requires higher V_C for ferroelectric switching since a thickness-independent electric field is needed to polarize the FE-Org barrier. In addition, by extrapolating V_C *vs.* t with linear fitting, one can see that a critical V_C of 0.2V is required even when the P(VDF-TrFE) thickness meets zero. This could reflect the ferroelectric-stiffen effect[30] due to the FM/FE-Org interface, where a supplementary energy barrier for switching is created due to the hybridization of the interfacial density of states.[3]

To check the homogeneity in ferroelectric polarization switching, the PFM phase maps were recorded on the *thin* and *medium* P(VDF-TrFE) surfaces (Figure 4c and 4d, respectively). The total images were scanned over 500× 500 nm^2 area. As shown in Figure 4c,d, the film was firstly polarized with a biased tip at positive voltage (+2V or +2.5V)[31] over an area of 300×300 nm^2, then an opposite poling bias (-2V or -2.5V) was subsequently applied over an area of 150×150 nm^2 in the middle of the previously polarized area. For the *thin* sample (Figure 4c), although a homogenous switching is found in the -2V polarizing area, inhomogeneous switching revealed by dark cycles is very evident in the zone of +2V polarizing area. More interestingly, the

size of the dark zones well corresponds to the size of P(VDF-TrFE) needle-like grains (see Figure 1b). This indicates that each P(VDF-TrFE) crystallite grain can act as a ferroelectric domain, and some grains are difficult to be positively polarized. On the contrary, the *medium* sample (Figure 4d) shows a rather homogenous phase map in positive and negative polarizing areas. These results clearly suggest a P(VDF-TrFE) thickness dependent ferroelectricity switching behavior.

As shown in Figure 2c, the thickness of P(VDF-TrFE) at "pot-hole" is much thinner than the mean barrier thickness. In fact, when P(VDF-TrFE) layer is very thin, the interface-induced ferroelectric polarization locking effect[32] can play an important role to produce an asymmetric ferroelectric switching and hinder the ferroelectric domain propagation crossing the "pot-hole" structures during sideway domain growth.[33] Therefore, the "pot-hole" structure could create the ferroelectric "ailing channel" and effectively influence the ferroelectric switching behavior. In Figure 4c, one can identify the "pot-hole" structure in the zone between the two unpolarized grains (indicated with red arrow), where the positive polarization state is not completely achieved. Our previous *ab initio* calculation[3] reveals that the F-C-H/Co interface in negatively polarized state is energetically favored (~25meV) than the H-C-F/Co interface in positively polarized state. This is due to the larger hybridization when the positively charged H atoms are closest to Co surface (F-C-H/Co). This can explain why a homogenous negatively polarized state can be achieved, while the positively polarized state is quite inhomogeneous.

Magneto-transport study of OMFTJs.

To study the influence of ferroelectric "ailing-channels" on the transport properties, the OMFTJ devices with different P(VDF-TrFE) thicknesses have been fabricated. The device structure is schematically shown in Figure 5a. Please see Experimental section for detailed fabrication procedure. To check the possibility of the existence of pinhole (direct metallic contact between top and bottom electrodes) to dominate the transport properties, we have performed conductive-AFM scanning at RT on the surface of organic barrier with different

thicknesses. With an applied voltage of +5V, no obvious leakage current conduction can be found (See Supporting Information S4). In addition, the resistances of OMTJs show an exponential increase with the increase of barrier thickness with a non-linear *I-V* characteristic for all devices (see Supporting Information S4). Together with the results from TEM observation, we can thus conclude that the pinhole does not play a role in our OMTJ devices.

Figure 5b shows the magneto-response (resistance *vs.* magnetic field) of the *medium* OMFTJ for two different ferroelectric polarizations (polarized using +2V and -2V, respectively) measured at 20K. Here, the TMR is defined as: $TMR = \frac{R_{AP}-R_P}{R_P} \times 100\%$ for positive TMR, and $TMR = \frac{R_{AP}-R_P}{R_{AP}} \times 100\%$ for negative TMR, where R_P and R_{AP} are junction resistance when the magnetizations of two electrodes are parallel and antiparallel, respectively. The TER is defined as: $TER = \frac{R_P^{Down}-R_P^{Up}}{R_P^{Up}} \times 100\%$, where R_P^{Down} and R_P^{Up} are parallel resistance in P(VDF-TrFE) "down" and "up" polarization states, respectively. In our case, the "down" and "up" polarization states correspond to the conditions when P(VDF-TrFE) barrier is polarized with positive and negative polarizing voltages, respectively. One can clearly notice that with the same bias voltage (+10mV), a positive +3.6% TMR or a negative -11.5% TMR can be achieved when the P(VDF-TrFE) is polarized to "down" state or "up" state, respectively. Simultaneously, a huge difference between the two parallel resistances (R_P) for the two polarizations allows to reach a TER over 600%. The four resistance states associated with different magnetization and ferroelectric configurations are identified in the inset of Figure 5b. Similar to our previous work with a PVDF organic barrier, the inverse of the TMR when P(VDF-TrFE) ferroelectric polarization is switched can be attributed to the change of spin-polarization sign at Co/P(VDF-TrFE) interface.[3] Compared to the pure PVDF system,[3] OMFTJs based on P(VDF-TrFE) show a comparable TMR effect, but much larger TER effect, proving an advanced ferroelectricity of the P(VDF-TrFE) copolymers.

To compare with devices with different P(VDF-TrFE) thicknesses, we show the magneto-response curves of the *thin*, *medium* and *thick* OMFTJs in Figure 5c-e, respectively. It is interesting to find that although the

TMR effect is reduced in the *thick* device (~2%), the TMR sign can still be changed by switching the P(VDF-TrFE) polarization. However, for the *thin* device, the TMR sign cannot be changed and only a modulation of TMR amplitude (from -19.1% to -2.4%) is found. To further prove that the TMR sign change or amplitude modulation is correlated to the change of P(VDF-TrFE) polarization, the parallel resistance (R_p) and the TMR are measured as a function of the polarizing voltage, as shown in Figure 5f-k for different thickness devices. In the three cases, the resistances measured at 20K clearly show hysteresis loop behaviors with coercive voltages (V_C) larger than those measured by PFM on the full P(VDF-TrFE) films at RT. We also plot V_C *vs. t* in Figure 4b and find that the linear fitting of V_C *vs. t* can lead to a same value of 0.2V as extracted from PFM results when the P(VDF-TrFE) thickness meets zero. This validates that the resistance change is indeed resulted from the P(VDF-TrFE) barrier itself and excludes the possibility of resistivity switching resulted from the change of LSMO surface due to the migration of oxygen vacancy.[34,35] From the TMR loops of the *medium* and *thick* OMFTJs, one can see that the sign of TMR closely depends on the ferroelectric state of P(VDF-TrFE). The positive TMR is associated with the high resistance state, while the negative TMR is linked to the low resistance state. The TMR loop processes exact the same V_C as the R_p loop. For the *thin* device, the TMR loop is also correlated with the resistance loop, *i.e.* the low TMR is associated with the high resistance state, while the high TMR is linked to the low resistance state. Especially, we show respectively two loops of measurements for R_p and TMR in Figure 5f,g and 5i,j, which can be well repeated. This is completely different from the mechanism of the change of TMR sign due to the formation of pinholes.[35,36] The latter case normally shows a random feature for TMR sign change which cannot be correlated with the loop of junction resistivity. Therefore, our results provide a strong argument that the sign or modulation of TMR is controlled by the ferroelectric polarization of the P(VDF-TrFE) barrier.

The aforementioned ferroelectric “ailing-channels” can help us to decipher the reason behind the nonswitchable TMR sign for the *thin* device upon the P(VDF-TrFE) polarization. Firstly, the TER in the *thin*

device is only about 30% at 20K, which is much lower than that of *medium* (600%) and *thick* (145%) devices, as seen in Figure 5f-h. This undoubtedly indicates a partial ferroelectric polarization in the *thin* organic barrier. Secondly, due to the existence of ferroelectric "ailing-channels" in the "pot-hole" structures, it has been seen in the PFM phase map (Figure 4c) that an important inhomogeneity of ferroelectric polarization exists in the +2V polarizing area while a relatively good homogeneity of negative polarization state appears in the -2V polarizing area. This means that with -2V polarizing voltage the *thin* device can almost reach fully negatively polarized state, but +2V polarizing voltage is not sufficient to fully positively polarize all ferroelectric domains. Since the junction size ($200\times200\mu m^2$) is much larger than the ferroelectric domain size (≈grain size $100\times50nm^2$), the TMR is determined by the average spin polarization at Co/P(VDF-TrFE) interface within the junction area. As a consequence, a large negative TMR of -19% is obtained with fully negatively polarized state while a much smaller TMR of -2.4% is measured with partially positively polarized state. Since the electrons are inclined to transport through the thinnest parts in the P(VDF-TrFE) barrier, a large portion of electrons probably tunnels through the "pot-hole" structure and contribute to the TMR and TER effects. This emphasizes the critical role of "pot-hole" structure on the spin-transport properties. To avoid creating ferroelectric "ailing channels" in the "pot-hole" structure to hinder the effective polarization switching like in the *thin* device case, it is important to improve the organic barrier surface roughness and eliminate the "pot-hole" structure substantially. Other growth method such as Langmuir-Blodgett method[37] will be tried in the future to grow thin organic barrier layer.

In the last part, the results for the temperature dependence of TER and TMR (Figure 6a-c) are reported for the devices with different P(VDF-TrFE) thicknesses. For the three samples, we have firstly ferroelectrically polarized P(VDF-TrFE) in two polarization states at 20K, and then increased the temperature separately. It is found that the TER in all samples decreases with increasing temperature. The *medium* device shows a lowest decay rate and still remains 200% TER at RT (Figure 6b). For the three samples, the TMR in both polarization

states decreases monotonously with the increase of temperature (Figure 6a-c). The decrease of TMR with temperature cannot be ascribed only to the loss of LSMO surface magnetization at room temperature,[38] but also strongly depends on the P(VDF-TrFE) thickness. The TMR in the *thick* device vanishes above 100K (Figure 6c), while the TMR in the *thin* and *medium* devices is still measurable above 250K (Figure 6a,b). The thickness dependent TMR allows us to extract the spin diffusion length for spin-polarized electron transport through the P(VDF-TrFE) organic barrier. The inset of Figure 6d presents the TMR in negative polarization as a function of P(VDF-TrFE) thickness measured at 20K. The exponential decay of TMR *vs. t* can be fitted with the Jullière formula:[24,27,39]

$$\frac{\Delta R}{R} = \frac{2P_1P_2e^{-(t-t_0)/\lambda_s}}{1-P_1P_2e^{-(t-t_0)/\lambda_s}} \qquad (1)$$

Where P_1 and P_2 are spin-polarizations of the Co/P(VDF-TrFE) and P(VDF-TrFE)/LSMO interface, respectively. t is the mean thickness of organic layer and t_0 is the "ill-defined" layer at the FM/FE-Org interface due to the metal penetration,[27] which can be neglected in our case due to the very limited Co diffusion in P(VDF-TrFE). λ_S is the spin diffusion length. As shown in the inset of Figure 6d, the fitting is quite good, which gives a product of P_1P_2 to be about 0.28±0.01 and λ_S to be about 7.2±0.2nm. Considering that the spin-polarization of bulk Co is about 0.43[40] and LSMO is close to 1 at 20K,[41] the fitted results are quite reasonable. The spin diffusion length found in the P(VDF-TrFE) is much smaller than those reported in Alq3 (45nm)[24] and P(NDI2OD-T2) (65nm)[27] measured at 4.2K. This could be a result of the enhanced spin relaxation due to the presence of high dielectric field inside the ferroelectric organic barrier. Furthermore, we plot the temperature dependence of the spin diffusion length as a function of temperature in Figure 6d. The spin diffusion length decreases very slightly from 7.2nm at 20K to 6nm at 80K, and the interface spin polarization almost remains constant. The spin relaxation time can also be extracted from $\tau_s=e\lambda_s^2/kT\mu$,[42] where k is Boltzmann constant and μ is mobility. By taking account of the mobility μ about 7.3×10^{-3}cm^{2}V^{-1}s^{-1} measured in the P(VDF-TrFE)

based ferroelectric organic memory transistor[43] and assuming that the mobility is temperature independent, the spin relaxation time τ_s can be estimated to be about 41ns at 20K and 7ns at 80K.

Conclusions

In summary, OMFTJs based on $La_{0.6}Sr_{0.4}MnO_3$/P(VDF-TrFE)/Co structures with different thickness of P(VDF-TrFE) have been studied. The combined STEM imaging and EELS spectroscopy analyses clearly show a very limited diffusion of Co into the P(VDF-TrFE) organic barrier when top electrode is deposited at low temperature. Pot-hole structures at the boundaries of the P(VDF-TrFE) grains have been evidenced to induce ferroelectric "ailing-channels" that hinder efficiently polarizing the organic barrier and quench the spin polarization switching at Co/P(VDF-TrFE) interface. As a consequence, the TMR sign of OMFTJ changes in the thick device (t≥19nm), but no change of TMR sign is observed in the thin device (t≤15nm). Furthermore, the spin diffusion length in negatively polarized P(VDF-TrFE) is measured to be about 7.2nm at 20K. This study highlights the interplay of the ferroelectricity of the FE-Org barrier with the spin transport properties of the OMFTJ and paves a comprehensive way to optimize the conditions for ferroelectric control of spin polarization of "spinterface".

Experimental Section

Sample preparation.

OMFTJ samples based on LSMO/P(VDF-TrFE)/Co structure were fabricated with different thickness of P(VDF-TrFE) as tunneling layer. The sample structure is shown in Figure 1a. $La_{0.6}Sr_{0.4}MnO_3$ film with thickness of ~85 nm was firstly epitaxial grown on <100> oriented $SrTiO_3$ (STO) substrates at 750°C using DC magnetron sputtering. The film was subsequently annealed at 800°C for two hours in O_2 atmosphere before being slowly cooled down to the room temperature. The P(VDF-TrFE) films were prepared by spin-coating method. The solutions were first obtained by dissolving P(VDF-TrFE) (VDF/TrFE=70/30) powders

(purchased from Piezotech-Arkema) into N,N-dimethylformamide (DMF) (purchased from Sigma-Aldrich). The solution was then spin-coated onto the LSMO/STO(001) substrate with a speed of 3000 RPM for 1min. Subsequently, the as-coated film was annealed at 150°C in air for two hours to improve the crystallinity of the ferroelectric β phase. The thickness of the P(VDF-TrFE) film is controlled by adjusting the concentration of the DMF:P(VDF-TrFE) solution (from 20 to 40mg/ml). The top Au/Co electrodes were deposited in a MBE system (with a base pressure of 1×10^{-10} torr) by e-beam evaporation. In the purpose of minimizing the metal diffusion into organic materials, the temperature during the growth of the top electrode is maintained at ~80K, by using liquid-N_2 cooling deposition technique. For the devices prepared for transport measurement, the $La_{0.6}Sr_{0.4}MnO_3$ layer was etched by using hydrogen chloride (37%) to pattern 200μm width bars as the bottom electrodes. After spin coating P(VDF-TrFE) layer, the 10nm Co/10nm Au was deposited in MBE with a shadow mask to form the top electrode. The final junction size is $200\times200\mu m^2$, as schematically shown in Figure 5a.

Piezo-response force microscopy characterization.

To check the ferroelectric properties of the P(VDF-TrFE) film with PFM, the P(VDF-TrFE) film was spin-coated on a thermal oxidized SiO_2/n-Si substrate covered with 100nm Au. The surface morphology was studied using an AFM (Asylum Research, MFP-3D, USA) working in contact mode under environmental conditions. Local electrical experiments were performed by using dual AC resonance tracking (DART) PFM. Ti/Ir conductive coating tips (Asylum Research ASYELEC-01 probes, k ~2.8 N m^{-1}) and ground conductive bottom electrodes were used.

HR-STEM/EELS characterization.

HR-STEM combined with spatially resolved EELS was performed by using a probe-corrected microscope JEOL ARM200F (cold FEG) equipped with a GATAN GIF quantum energy filter to reveal the structure and element distribution in the FM/FE-Org interface. Due to the strong sensitivity of polymers to electron-beam

damages, the microscope was operated at 80kV and the temperature of the sample was held at 103K using a Gatan double-tilt liquid nitrogen cooling sample holder. High angle annular dark-field (HAADF), annular dark-field (ADF) and bright-field (BF) images were simultaneously recorded for structural study while only HAADF and ADF images were recorded during EELS mapping. The spatial resolution of EELS maps is about 0.5 nm. During the spectrum image recording, the spatial drift was measured at the end of each line and a drift correction was immediately applied. This STEM-EELS combined chemical analysis technique has already been successfully employed to study interlayer chemical inter-diffusion in the spin-injector on spin light emitting diode at atomic-scale level.[44] The cross-sections for STEM observations were prepared by lift out method using a FIB FEI Helios NanoLab DualBeam.

Magneto-transport measurement.

The magneto-transport measurement was performed in a close cycle cryostat by varying temperature from 20K to 300K with magnetic field up to 4kOe. *I-V* measurements were performed in two-terminal geometry by using a Keithley 2400 as a voltage source and a Keithley 6487 picoammeter to measure the current. To polarize P(VDF-TrFE) barrier, electrical voltage pulse with a ramp of 0.1V/s and a duration of 1s was applied to the junction with different voltages. We have verified with conductive AFM that the polarizing voltage around ±2V range does not induce a damage of organic barrier with the formation of pinholes and leakage currents.

Supporting Information

In the Supporting Information, top electrode deposition with Liq-N_2 cooling technique, STEM and EELS mapping on the *medium* P(VDF-TrFE) sample, EDS characterization on the *thin* P(VDF-TrFE) sample, verification of pinhole contribution and anisotropic magnetoresistance in the ferromagnetic electrodes are described.

Acknowledgements

The authors thank Dr. A. Da Costa for technical support on AFM experiments. This work is supported by the joint French National Research Agency (ANR)-National Natural Science Foundation of China (NSFC) ENSEMBLE Project (Grant Nos. ANR-14-0028-01 and NNSFC 61411136001) and by the French PIA project "Lorraine Université d'Excellence", reference ANR-15-IDEX-04-LUE. The work at USTC was supported by NSFC (Grant No. 51790491) and National Key Research and Development Program of China (Grant No. 2016YFA0300103). The Région Hauts-de-France and the FEDER (EU) under the CPER project "Chemistry and Materials for a Sustainable Growth" is acknowledged for the funding of MFP-3D microscope. Experiments were performed using equipment from the platform TUBE-Davm funded by FEDER (EU), ANR, the Region Lorraine and Grand Nancy.

Figures

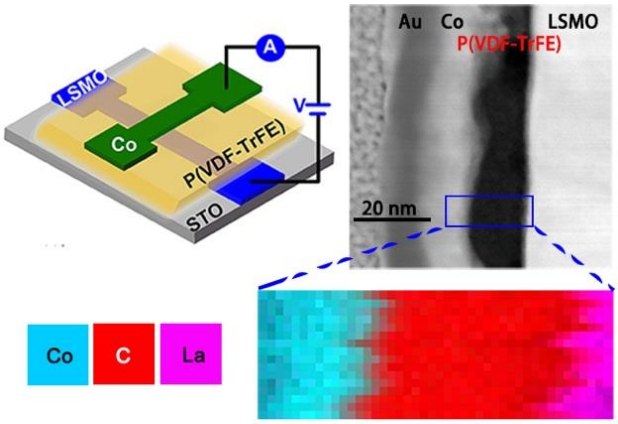

TOC figure: Schematics of the LSMO/P(VDF-TrFE)/Co device. STEM combined with EELS analysis was performed to study the structure and chemical distribution. Chemical map was extracted from the EELS spectrum image to display the distribution of Co, C and La elements in the blue rectangle area.

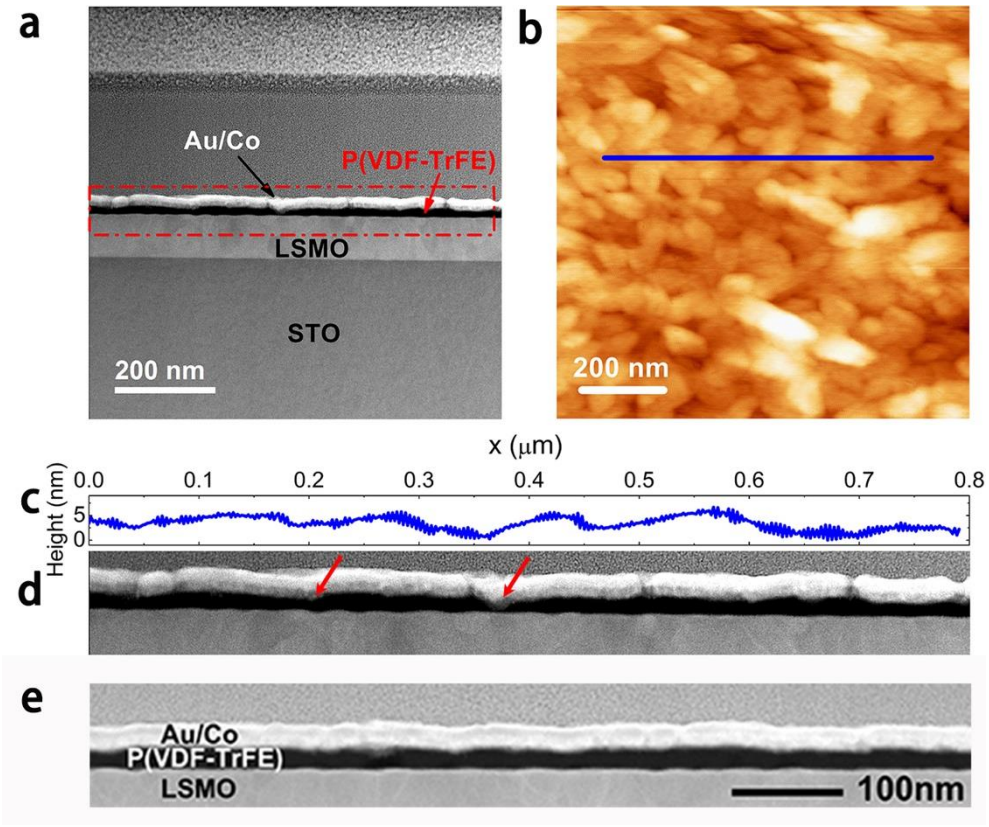

Figure 1. Morphology observation by STEM and AFM. (a) HAADF STEM image of LSMO/P(VDF-TrFE)(*t*=15nm)/Co sample. (b) AFM topography measurement of the P(VDF-TrFE) (*t*=15nm) barrier surface over 1×1 μm^2 area. (c) Section profile recorded by AFM along the blue line marked in (b). (d) Zoom-in of STEM image in the red dash rectangular area marked in (a). The red arrows indicate the "pot-hole" structures in the organic barrier. The width of the rectangular image is 0.8 μm. (e) HAADF STEM image of LSMO/P(VDF-TrFE)(*t*=19nm)/Co sample.

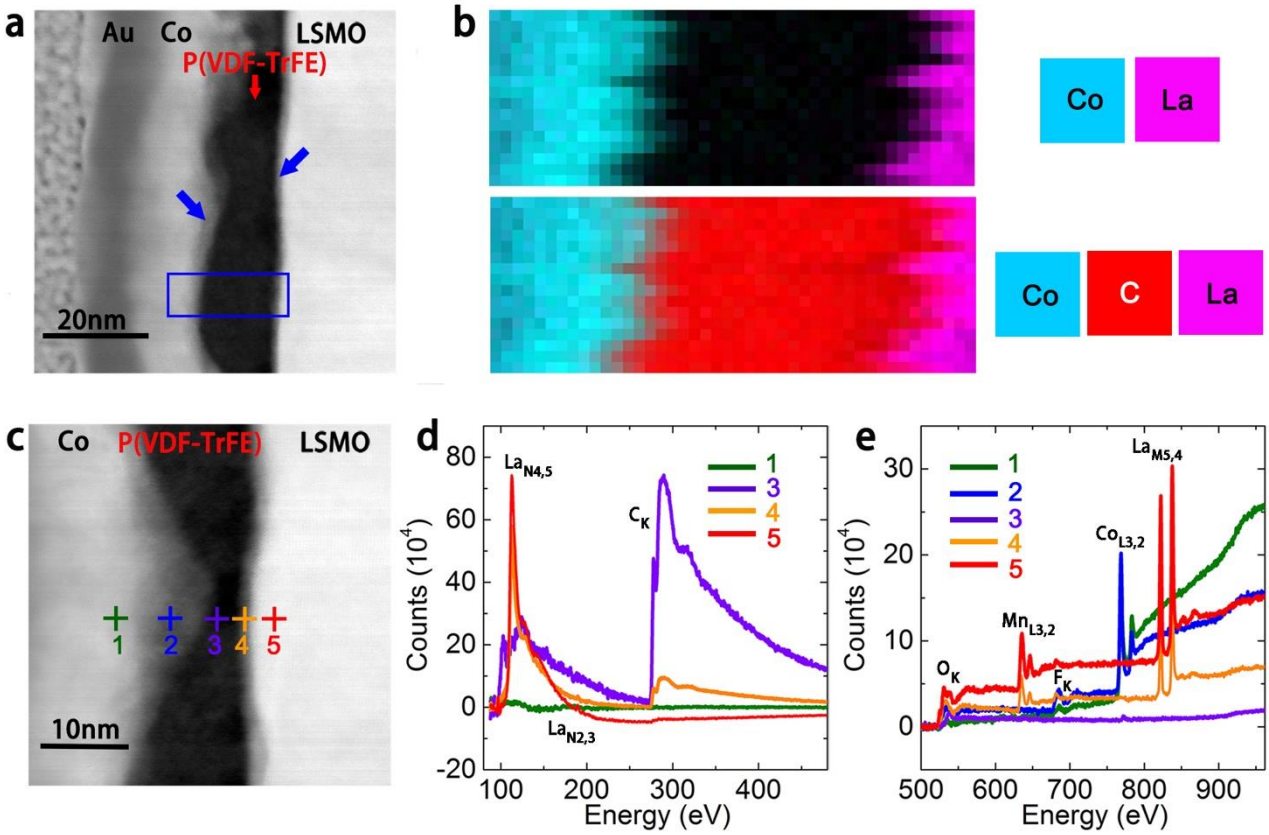

Figure 2. Chemical distribution analysis by STEM-EELS characterization. (a) ADF STEM image of LSMO/P(VDF-TrFE)(*t*=15nm)/Co sample. Blue arrows indicate the superposition zones due to the roughness of Co/P(VDF-TrFE) interface and P(VDF-TrFE)/LSMO interface. (b) Chemical maps drawn with Co_{L3}, C_K and La_{M5} signals extracted from the EELS spectrum image recorded in the blue rectangle area in (a). The corresponding colors assigned to the elements are labeled on the right of the images. (c) ADF STEM image of a zone where P(VDF-TrFE) grains form a "pot-hole" structure. (d-e) EELS spectra analysis recorded on different positions marked in (c).

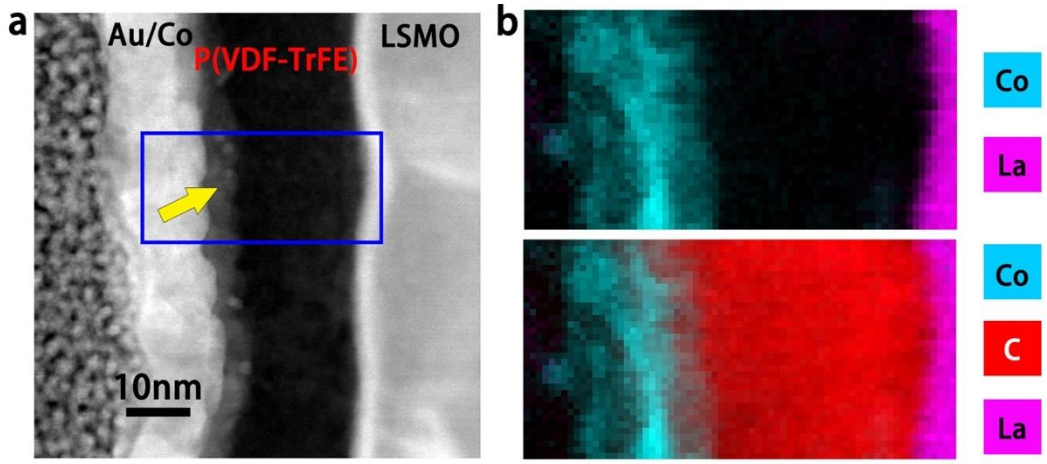

Figure 3. STEM-EELS characterization on the OMFTJ with the top electrode grown at RT. (a) HAADF STEM image of LSMO/P(VDF-TrFE)(*t*=19nm)/Co sample, whose Au/Co top electrode was grown at RT. Yellow arrow indicates the inter-diffusion zone. (b) Chemical maps drawn with Co_{L3}, C_K and La_{M5} signals extracted from the EELS spectrum image recorded in the blue rectangle area in (a).

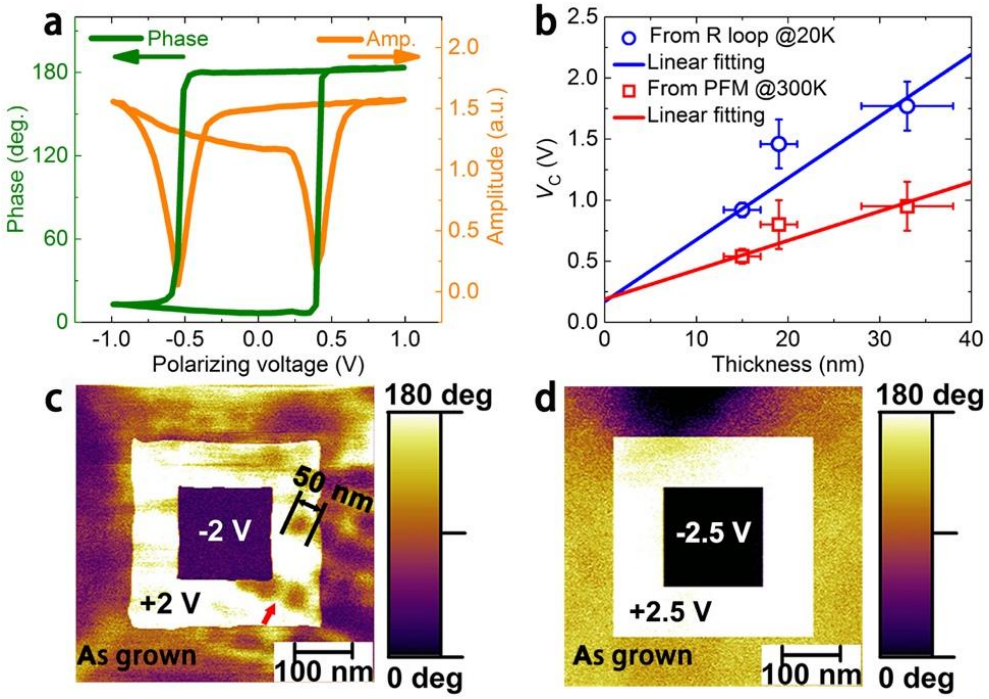

Figure 4. Ferroelectricity behaviors of P(VDF-TrFE) barriers. (a) Local PFM hysteresis phase and amplitude loops measured on the *thin* P(VDF-TrFE) surface (15nm) at RT. (b) Thickness dependence of polarizing voltage coercivity (V_C) of P(VDF-TrFE). The red squares show polarizing voltage coercivity measured by PFM at RT. The blue cycles show ferroelectric coercivity extracted from loops of R_P of LSMO/P(VDF-TrFE)(*t*)/Co devices measured at 20K. (c-d) PFM phase image recorded on the surface of *thin* and *medium* P(VDF-TrFE) samples, respectively. Contrasts show that the ferroelectric switching are firstly obtained after polarizing with +2 V (+2.5V) DC bias on the tip over 300×300 nm^2 (bright square) and subsequently polarizing with –2V (-2.5V) over inside 150×150 nm^2 area (dark square). The total image was acquired over 500×500 nm^2 area. The red arrow in (c) indicates the unpolarized zone in the "pot-hole" structure.

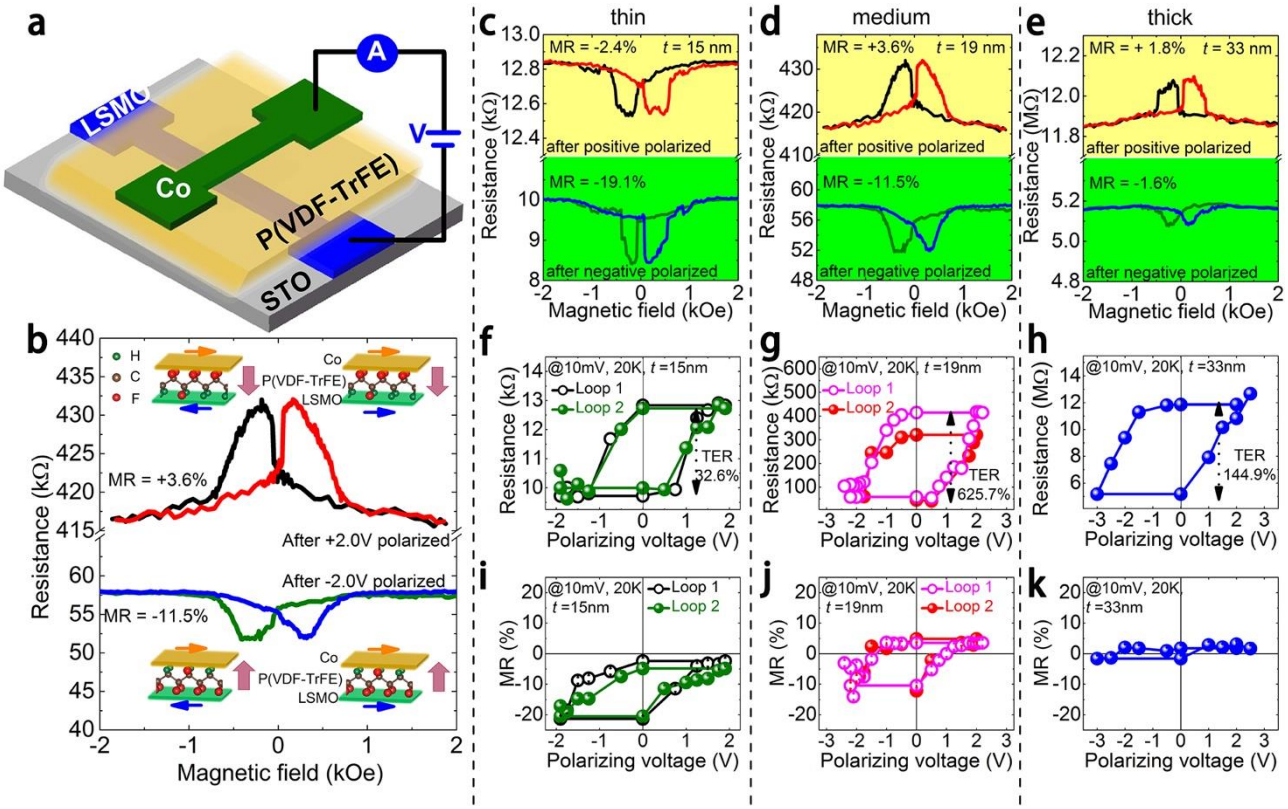

Figure 5. Magneto-transport measurements on LSMO/P(VDF-TrFE)/Co devices. (a) Schematics of the LSMO/P(VDF-TrFE)/Co device. (b) Magneto-response curves measured under a bias of +10mV at 20 K after +2.0 V and –2.0 V polarizing the device with 19nm thick P(VDF-TrFE). The insert schematics show four resistance states associated with different polarization and magnetization orientations. (c-e) Magneto-response curves measured under a bias of +10 mV at 20 K after negative and positive polarizing the devices with 15nm, 19nm and 33nm thick P(VDF-TrFE) layers, respectively. (f-h) Loops for parallel resistance versus electric polarizing voltage for the devices with 15nm, 19nm, and 33nm thick P(VDF-TrFE) layers, respectively. (i-k) Loops for TMR versus electric polarizing voltage for the devices with 15nm, 19nm and 33nm thick P(VDF-TrFE) layers, respectively.

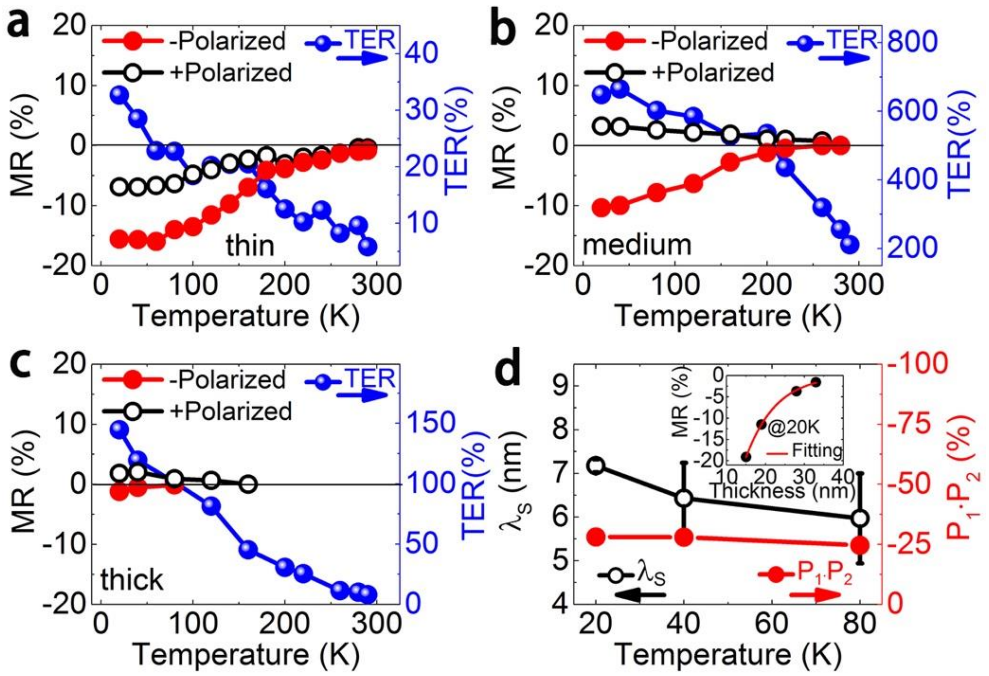

Figure 6. Temperature dependence of TER and TMR. (a-c) Temperature dependent TMR after negative and positive polarizing, for the devices LSMO/P(VDF-TrFE)(*t*)/Co, *t*=15nm, 19nm and 33nm, respectively. The blue curves show the temperature dependence of TER. (d) Temperature dependence of spin diffusion length and interface spin polarization product. Inset: TMR after negative polarizing measured at 20K with different thickness of P(VDF-TrFE). The red line is the fitting of data based on Eq. (1).

References and Notes:

1. Lopez-Encarnacion, J. M.; Burton, J. D.; Tsymbal, E. Y.; Velev, J. P. Organic Multiferroic Tunnel Junctions with Ferroelectric Poly(vinylidene fluoride) Barriers. *Nano Lett.* **2011**, *11*, 599-603

2. Velev, J. P. ; Lopez-Encarnacion, J. M.; Burton, J. D.; Tsymbal, E. Y. Multiferroic tunnel junctions with poly(vinylidene fluoride). *Phys. Rev. B* **2012**, *85*, 125103.

3. Liang, S.; Yang, H.; Yang, H.; Tao, B.; Djeffal, A.; Chshiev, M.; Huang, W.; Li, X.; Ferri, A.; Desfeux, R.; Mangin, S.; Lacour, D.; Hehn, M.; Copie, O.; Dumesnil, K.; Lu, Y. Ferroelectric Control of Organic/Ferromagnetic Spinterface. *Adv. Mater.* **2016**, *28*, 10204-10210.

4. Barraud, C.; Seneor, P.; Mattana, R.; Fusil, S.; Bouzehouane, K.; Deranlot, C.; Graziosi, P.; Hueso, L.; Bergenti, I.; Dediu, V.; Petroff, F.; Fert A. Unravelling the role of the interface for spin injection into organic semiconductors. *Nat. Phys.* **2010**, *6*, 615-620.

5. Dediu, V. A.; Hueso, L. E.; Bergenti, I.; Taliani, C. Spin routes in organic semiconductors. *Nat. Mater.* **2009**, *8*, 707-716.

6. Szulczewski, G.; Sanvito, S.; Coey, J. M. D. A spin of their own. *Nat. Mater.* **2009**, *8*, 693-695

7. Gajek, M.; Bibes, M.; Fusil, S.; Bouzehouane, K.; Fontcuberta, J.; Barthélémy, A.; Fert, A. Tunnel Junctions with Multiferroic Barriers. *Nat. Mater.* **2007**, *6*, 296-302.

8. Garcia, V.; Bibes, M.; Bocher, L.; Valencia, S.; Kronast, F.; Crassous, A.; Moya, X.; Enouz-Vedrenne, S.; Gloter, A.; Imhoff, D.; Deranlot, C.; Mathur, N. D.; Fusil, S.; Bouzehouane, K.; Barthélémy, A. Ferroelectric Control of Spin Polarization. *Science* **2010**, *327*, 1106-1110.

9. Pantel, D.; Goetze, S.; Hesse, D.; Alexe, D. M. Reversible electrical switching of spin polarization in multiferroic tunnel junctions. *Nat. Mater.* **2012**, *11*, 289-293.

10. Garcia, V.; Bibes, M. Ferroelectric tunnel junctions for information storage and processing. Ferroelectric tunnel junctions for information storage and processing. *Nat. Commun.* **2014**, *5*, 4289.

11. Tsymbal, E. Y.; Kohlstedt, H. Tunneling across a Ferroelectric. *Science* **2006**, *313*, 181-183.

12. Velev, J. P.; Duan, C.-G.; Burton, J. D.; Smogunov, A.; Niranjan, M. K.; Tosatti, E.; Jaswal, S. S.; Tsymbal, E. Y. Magnetic Tunnel Junctions with Ferroelectric Barriers: Prediction of Four Resistance States from First Principles. *Nano Lett.* **2009**, *9*, 427-432.

13. Scott, J. F. Data storage: Multiferroic memories. *Nat. Mater.* **2007**, *6*, 256-257.

14. Sanvito, S. The rise of spinterface science. *Nat. Phys.* **2010**, *6*, 562-564.

15. Liang, S.; Liu, D.; Tao, L.; Han, X. F.; Guo, H. Organic magnetic tunnel junctions: The role of metal-molecule interface. *Phys. Rev. B* **2012**, *86*, 224419.

16. Liang, S.; Geng, R.; Yang, B.; Zhao, W.; Subedi, R. C.; Li, X. G.; Han, X. F.; Nguyen, T. D. Curvature-enhanced Spin-orbit Coupling and Spinterface Effect in Fullerene-based Spin Valves. *Sci. Rep.* **2016**, *6*, 19461.

17. Djeghloul, F.; Ibrahim, F.; Cantoni, M.; Bowen, M.; Joly, L.; Boukari, S.; Ohresser, P.; Bertran, F.; Le Fevre, P.; Thakur, P.; Scheurer, F.; Miyamachi, T.; Mattana, R.; Seneor, P.; Jaafar, A.; Rinaldi, C.; Javaid, S.; Arabski, J.; Kappler, J. -P.; Wulfhekel, W.; Brookes, N. B.; Bertacco, R.; Taleb-Ibrahimi, A.; Alouani, M.; Beaurepaire, E.; Weber, W. Direct observation of a highly spin-polarized organic spinterface at room temperature. *Sci. Rep.* **2013**, *3*, 1272.

18. Kim, K. L.; Lee, W.; Hwang, S. K.; Joo, S. H.; Cho, S. M.; Song, G.; Cho, S. H.; Jeong, B.; Hwang, I.; Ahn, J.-H.; Yu, Y.-J.; Shin, T. J.; Kwak, S. K.; Kang, S. J.; Park. C. Epitaxial Growth of Thin Ferroelectric Polymer Films on Graphene Layer for Fully Transparent and Flexible Nonvolatile Memory. *Nano Lett.* **2016**, *16*, 334–340.

19 . Jo, J.; Choi, W. Y.; Park, J.-D.; Shim, J. W.; Yu, H.-Y.; Shin, C. Negative Capacitance in Organic/Ferroelectric Capacitor to Implement Steep Switching MOS Devices. *Nano Lett.* **2015**, *15*, 4553–4556.

20. Asadi, K.; de Leeuw, D. M.; de Boer, B.; Blom, P. W. M. Organic non-volatile memories from ferroelectric phase-separated blends. *Nat. Mater.* **2008**, *7*, 547–550.

21. Naber, R. C. G.; Asadi, K.; Blom, P. W. M.; de Leeuw, D. M.; de Boer, B. Organic nonvolatile memory devices based on ferroelectricity. *Adv. Mater.* **2010**, *22*, 933–945.

22. Tian, B. B.; Wang, J. L.; Fusil, S.; Liu, Y.; Zhao, X. L.; Sun, S.; Shen, H.; Lin, T.; Sun, J. L.; Duan, C. G.; Bibes, M.; Barthélémy, A.; Dkhil, B.; Garcia, V.; Meng, X. J.; Chu, J. H. Tunnel electroresistance through organic ferroelectrics. *Nat. Commun.***2016**, *7*, 11502.

23. Mabuchi, Y.; Nakajima, T.; Furukawa, T.; Okamura, S. Electric-field-induced polarization enhancement of vinylidene fluoride/trifluoroethylene copolymer ultrathin films. *App. Phys. Exp.* **2011**, *4*, 071501.

24 Xiong, Z. H.; Wu, D.; Vardeny, Z. V.; Shi, J. Giant magnetoresistance in organic spin-valves. *Nature* **2004**, *427*, 821-824.

25. Sun, D.; Yin, L.; Sun, C.; Guo, H.; Gai, Z.; Zhang, X.-G.; Ward, T. Z.; Cheng, Z.; Shen, J. Giant Magnetoresistance in Organic Spin Valves. *Phys. Rev. Lett.* **2010**, *104*, 236602.

26. Venkatesan, M.; Tokuch, H.; Burke, F.; Szulczewski, G.; Coey, J. M. D. Magnetic properties of ultrathin tetragonal Heusler $D0_{22}$-Mn_3Ge perpendicular-magnetized films. *J. Appl. Phys.* **2011,** *109*, 07C507.

27. Li, F.; Li, T.; Chen, F.; Zhang F. P. Excellent spin transport in spin valves based on the conjugated polymer with high carrier mobility. *Sci. Rep.* **2015**, *5*, 9355.

28. Jang, H.-J.; Richter, C. A. Organic Spin-Valves and Beyond: Spin Injection and Transport in Organic Semiconductors and the Effect of Interfacial Engineering. *Adv. Mater.* **2017**, *29*, 1602739.

29. Subedi, R. C.; Geng, R.; Luong, H. M.; Huang, W.; Li, X.; Hornak, L. A.; Nguyen, T. D. Large magnetoelectric effect in organic ferroelectric copolymer-based multiferroic tunnel junctions. *Appl. Phys. Lett.* **2017**, *110*, 053302.

30. O'Callaghan, M. J. Polarization-stiffened ferroelectric liquid crystals: A thickness-independent bistable switching voltage with a lower limit of about 2V and the transition to thresholdless switching. *Phys. Rev. E* **2015**, *91*, 022502

31. The slight higher polarizing voltage (±2.5V) employed for the *medium* sample is proportional to the thickness of P(VDF-TrFE) barrier in comparison to the *thin* sample.

32. Han, M.-G.; Marshall, M. S. J.; Wu, L.; Schofield, M. A.; Aoki, T.; Twesten, R.; Hoffman, J.; Walker, F. J.; Ahn, C. H.; Zhu, Y. Interface-induced nonswitchable domains in ferroelectric thin films. *Nat. Commun.* **2014**, *5*, 4693

33. Hu, W.; Juo, D.-M.; You, L.; Wang, J.; Chen, Y.-C.; Chu, Y.-H.; Wu, T. Universal Ferroelectric Switching Dynamics of Vinylidene Fluoride-trifluoroethylene Copolymer Films. *Sci. Rep.* **2014**, *4*, 4772

34. Grünewald, M.; Homonnay, N.; Kleinlein, J.; Schmidt, G. Voltage-controlled oxide barriers in organic/hybrid spin valves based on tunneling anisotropic magnetoresistance. *Phy. Rev. B* **2014**, *90*, 205208.

35. Göckeritz, R.; Homonnay, N.; Müller, A.; Fuhrmann, B.; Schmidt, G. Resistive switching and voltage induced modulation of tunneling magnetoresistance in nanosized perpendicular organic spin valves, *AIP Adv.* **2016**, *6*, 045003.

36. Göckeritz, R.; Homonnay , N.; Müller, A.; Richter, T.; Fuhrmann, B.; Schmidt, G. Nanosized perpendicular organic spin-valves, *Appl. Phys. Lett.* **2015**, *106*, 102403.

37. Palto, S.; Blinov, L.; Bune, A.; Dubovik, E.; Fridkin, V.; Petukhova, N.; Verkhovskaya. K.; Yudin, S. Ferroelectric Langmuir-Blodgett films. *Ferroelectr. Lett.* **1995**, *19*, 65-68.

38. Park, J.-H.; Vescovo, E.; Kim, H.-J.; Kwon, C.; Ramesh, R.; Venkatesan, T. Magnetic Properties at Surface Boundary of a Half-Metallic Ferromagnet $La_{0.7}Sr_{0.3}MnO_3$. *Phys. Rev. Lett.* **1998**, *81*, 1953.

39. Julliere, M. Tunneling between ferromagnetic films. *Phys. Lett. A* **1975**, *54*, 225–226.

40. Tsymbal, E. Y.; Mryasov, O. N.; LeClair, P. R. Spin dependent tunnelling in magnetic tunnel junctions. *J. Phys.: Condens. Matter*. **2003**, *15*, R109–R142.

41. Garcia, V.; Bibes, M.; Barthélémy, A.; Bowen, M.; Jacquet, E.; Contour, J.-P.; Fert, A. Temperature dependence of the interfacial spin polarization of $La_{2/3}Sr_{1/3}MnO_3$. *Phys. Rev. B* **2004**, *69*, 052403.

42. Pramanik, S.; Stefanita, C.-G.; Patibandla, S.; Bandyopadhyay, S.; Garre, K.; Harth, N.; Cahay, M. Observation of extremely long spin relaxation times in an organic nanowire spin valve. *Nat. Nanotechnol.* **2007**, *2*, 216–219.

43. Kim, J.-H.; Bae, J.-H.; Kim, M.-H. Roughness Reduction of PVDF-TrFE Insulator by Reverse Transfer Printing for Enhanced Performance of Ferroelectric Organic Memory Transistors. *J. Nanosci. Nanotechnol.* **2017**, *17*, 4149-4152.

44. Tao, B.; Barate, P.; Devaux, X.; Renucci, P.; Frougier, J.; Djeffal, A.; Liang, S.; Xu, B.; Hehn, M.; Jaffres, H.; George, J.-M.; Marie, X.; Mangin, S.; Han, X.; Wang, Z.; Lu, Y. Atomic-scale understanding of high thermal stability of the Mo/CoFeB/MgO spin injector for spin-injection in remanence. *Nanoscale* **2018**, *10*, 10213-10220.